


Unconventional anomalous Hall effect from magnetization parallel to the electric field

 Hengxin Tan, Yizhou Liu, and Binghai Yan *

Department of Condensed Matter Physics, Weizmann Institute of Science, Rehovot 7610001, Israel

 (Received 2 May 2021; revised 25 May 2021; accepted 16 June 2021; published 22 June 2021)

In the anomalous Hall effect (AHE), the magnetization, electric field, and Hall current are presumed to be mutually vertical to each other. In this paper, we propose an unconventional AHE where the magnetization, electric field, and Hall current stay inside the same plane. Such an AHE is odd under time reversal and exists even when the magnetization is parallel to the electric field or Hall current, different from the planar Hall effect which is even under time reversal. Here, we term it parallel anomalous Hall effect (PAHE). We reveal that the PAHE exists when all the point group rotational and reflection symmetries are broken where the Berry curvature field is not necessarily parallel to the magnetization axis. We further demonstrate the PAHE in a ferrimagnetic Weyl semimetal FeCr₂Te₄.

 DOI: [10.1103/PhysRevB.103.214438](https://doi.org/10.1103/PhysRevB.103.214438)

I. INTRODUCTION

The intrinsic anomalous Hall effect (AHE) [1] is established on the Berry phase theory [2] and provides a powerful probe on the time-reversal breaking and the band topology. In general, it is presumed that three vectors—magnetization, electric field, and the Hall current—are mutually perpendicular to each other, which is like the conventional Hall effect in an external magnetic field. However, the recent discovery of giant AHE in noncollinear antiferromagnets [3–6] questioned this assumption, in which the net magnetization vanishes. Furthermore, the quantized AHE was theoretically proposed to exist with these three vectors being coplanar in some two-dimensional (2D) films that break all reflection symmetries [7–10]. It is elusive how this in-plane AHE is generalized to three-dimensional (3D) materials and what symmetry condition is required.

Here, we express the anomalous Hall current as $\mathbf{J}^{\text{AHE}} = \frac{e^2}{\hbar} \boldsymbol{\Omega} \times \mathbf{E}$, where $\boldsymbol{\Omega}$ is the total Berry curvature of the band structure, \mathbf{E} the applied electric field, and $\frac{e^2}{\hbar}$ the conductance quantum. If any rotational or reflection symmetry exists, both $\boldsymbol{\Omega}$ and the magnetization \mathbf{m} must lie parallel to the rotational axis or the reflection plane normal, because $\boldsymbol{\Omega}$ is a pseudospin-type vector. Therefore, \mathbf{J}^{AHE} , \mathbf{E} , and \mathbf{m} are mutually orthogonal in this case. However, if all rotational and reflection symmetries are broken, $\boldsymbol{\Omega}$ unnecessarily aligns along \mathbf{m} . Then the orthogonal relation may get violated. Three vectors, \mathbf{J}^{AHE} , \mathbf{E} , and \mathbf{m} can be coplanar and \mathbf{m} may even be parallel to \mathbf{J}^{AHE} or \mathbf{E} , as schematically shown in Fig. 1. We note this unconventional AHE as parallel anomalous Hall effect (PAHE). Like the conventional AHE, PAHE changes signs as reversing the \mathbf{m} direction. It is distinct from the planar Hall effect [11–14], which remains the same when flipping the magnetic field and originates in the anisotropic magnetoresistance.

In this paper, we investigate the PAHE in general 3D materials. We demonstrate the misalignment between magnetization and Berry curvature if anisotropic spin-orbit coupling (SOC) exists. Unlike the 2D case, we need to break all rotational and reflection symmetries except the spatial inversion to generate PAHE in 3D. We analyze all 32 point groups (PGs) and identify the allowed PAHE. Further, we propose the experimental available magnetic Weyl semimetal FeCr₂Te₄ as a candidate to realize PAHE.

II. A TOY MODEL

We first illustrate the PAHE by a simple two-band toy model in this section. The two-band anisotropic model Hamiltonian can be written as

$$\begin{aligned} H &= H_0 + H_Z + H_{\text{SO}}, \\ H_0 &= \frac{\hbar \mathbf{k}^2}{2m^*}, \quad H_Z = \mathbf{g} \mathbf{m} \cdot \boldsymbol{\sigma}, \\ H_{\text{SO}} &= \lambda_x k_x \sigma_x + \lambda_y k_y \sigma_y + \lambda_z k_z \sigma_z, \end{aligned} \quad (1)$$

where H_{SO} and H_Z are SOC and Zeeman-like terms, respectively. $\boldsymbol{\lambda} = (\lambda_x, \lambda_y, \lambda_z)$ refers to the SOC strength. $\boldsymbol{\sigma} = (\sigma_x, \sigma_y, \sigma_z)$ is the spin Pauli matrix and $\mathbf{m} = (m_x, m_y, m_z)$ is the magnetization. If $\lambda_x = \lambda_y = \lambda_z = \lambda$, H_{SO} is reduced to the ordinary isotropic form $\lambda \mathbf{k} \cdot \boldsymbol{\sigma}$. The Hamiltonian in Eq. (1) can be rewritten into a compact form $H = d_0 \sigma_0 + \mathbf{d} \cdot \boldsymbol{\sigma}$ (σ_0 is a 2×2 identity matrix) whose energy band dispersion is given by $\varepsilon_{s\mathbf{k}} = d_0 + s\sqrt{\mathbf{d} \cdot \mathbf{d}}$ ($s = \pm 1$) with $d_0 = \hbar^2 \mathbf{k}^2 / (2m^*)$ and $d_\alpha = \lambda_\alpha k_\alpha + g m_\alpha$ ($\alpha = x, y, z$). The total Berry curvature $\boldsymbol{\Omega}$ can be calculated as

$$\begin{aligned} \boldsymbol{\Omega}_{s\mathbf{k}} &= s \frac{\lambda_x \lambda_y \lambda_z}{2|\mathbf{d}|^3} (\mathbf{k} + \mathbf{g} \mathbf{m}_\lambda) \\ \boldsymbol{\Omega} &= \sum_{s=\pm} \int \frac{d\mathbf{k}}{(2\pi)^3} \boldsymbol{\Omega}_{s\mathbf{k}} f_{s\mathbf{k}} \\ &= \left(- \sum_{s=\pm} \int_{\varepsilon \leq \mu} \frac{d\mathbf{k}}{(2\pi)^3} s \frac{g \lambda_x \lambda_y \lambda_z}{2|\mathbf{d}|^3} \right) \mathbf{m}_\lambda, \end{aligned} \quad (2)$$

*binghai.yan@weizmann.ac.il

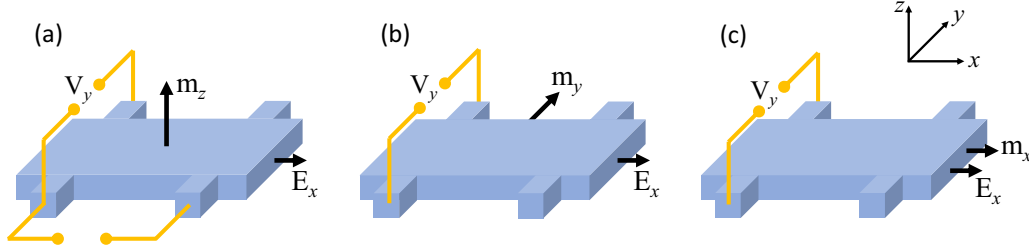


FIG. 1. Schematics of the anomalous Hall effect. (a) The standard Hall bar where the magnetization \mathbf{m} (or magnetic field \mathbf{H}) is along z , electric field \mathbf{E} is along x , and the Hall voltage V_y is measured along y . The general electric resistance can be obtained by measuring along x . (b) The \mathbf{m} (or \mathbf{H}) is along y . (c) The \mathbf{E} and \mathbf{m} are in the same direction x . The anomalous Hall effect along y (V_y) in (b) and (c) are PAHE, which vanishes in the conventional Hall effect and the planar Hall effect. We have to emphasize that the realization of (b) and (c) in real experiments can be achieved by preparing a new sample with the magnetization lying in the sample plane and applying \mathbf{E} parallel to or along with \mathbf{m} , instead of rotating \mathbf{m} from (a) directly.

where $\mathbf{m}_\lambda = (\frac{m_x}{\lambda_x}, \frac{m_y}{\lambda_y}, \frac{m_z}{\lambda_z})$. μ is the chemical potential. Equation (2) indicates that the direction of Berry curvature $\mathbf{\Omega}$ is parallel to the magnetization \mathbf{m} only in the isotropic case ($\mathbf{m}_\lambda = \mathbf{m}/\lambda$). For generic low-symmetry anisotropic SOC, \mathbf{m}_λ or $\mathbf{\Omega}$ is not necessarily collinear with \mathbf{m} . We have to emphasize that, while the simple Weyl Hamiltonian is used here to establish intuition on PAHE, the PAHE does not necessarily require the existence of Weyl points (WPs), as seen from the symmetry analyses below.

A similar conclusion also applies to the conventional Hall effect. Based on the Boltzmann transport theory, the conventional Hall current (\mathbf{J}^{HE}) due to Lorentz force can be derived as

$$\mathbf{J}^{\text{HE}} = -e^3 \tau^2 \int \frac{d\mathbf{k}}{(2\pi)^3} \mathbf{v}\mathbf{v} \cdot \left[\mathbf{B} \times \left(\frac{1}{m^*} \right) \mathbf{E} \right] \frac{\partial f_0}{\partial \varepsilon}, \quad (3)$$

where $(\frac{1}{m^*})_{\alpha\beta} = \frac{1}{\hbar^2} \frac{\partial^2 \varepsilon_{\mathbf{k}}}{\partial k_\alpha \partial k_\beta}$ is the inverse effective mass matrix and $\mathbf{v} = \frac{1}{\hbar} \nabla_{\mathbf{k}} \varepsilon_{\mathbf{k}}$ is the group velocity. f_0 is the equilibrium Fermi distribution function. In the case of an isotropic parabolic band with a constant effective mass, i.e., $\varepsilon_{\mathbf{k}} = \frac{\hbar^2 \mathbf{k}^2}{2m^*}$, the \mathbf{J}^{HE} can be calculated as $\mathbf{J}^{\text{HE}} = \sigma_H \mathbf{B} \times \mathbf{E}$ with $\sigma_H = \frac{e^3 \tau^2 n_F}{m^{*2}}$ (n_F is the carrier density at Fermi level). However, in the case of an anisotropic effective mass model, i.e., $\varepsilon_{\mathbf{k}} = \frac{\hbar^2 k_x^2}{2m_x^*} + \frac{\hbar^2 k_y^2}{2m_y^*} + \frac{\hbar^2 k_z^2}{2m_z^*}$, the Hall current becomes $\mathbf{J}^{\text{HE}} = \frac{e^3 \tau^2 n_F}{m_x^* m_y^* m_z^*} \mathbf{B} \mathbf{m}^* \times \mathbf{E}$ with $\mathbf{B} \mathbf{m}^* = (m_x^* B_x, m_y^* B_y, m_z^* B_z)$, so \mathbf{J}^{HE} is not necessarily perpendicular to \mathbf{B} .

III. SYMMETRY RESTRICTIONS ON ANOMALOUS HALL EFFECT

Our above discussions indicate that symmetry is a decisive factor for the appearance of PAHE. Let's now consider from a generic aspect how the symmetry restricts the AHE. In the experiment, the AHE is generally measured with magnetization \mathbf{m} or magnetic field \mathbf{H} along the high-symmetry directions. For this reason, and also for the sake of simplicity, we start from the 32 PGs and apply the magnetization \mathbf{m} along the three orthogonal axes of the Cartesian coordinate systems conventionally used for all crystal systems [15], as summarized in the Supplemental Material (SM) [16]. Note that for the trigonal crystal system, we employ the hexagonal lattice settings. The elements of the anomalous Hall conductivity

(AHC) tensor σ that allow PAHE are summarized in Table I after considering the symmetry broken by \mathbf{m} (more details can be found in the SM [16]). The PAHE is not allowed for (i) the five cubic PGs, (ii) the dihedral PGs except for D_3 and D_{3d} , and (iii) the C_{nv} PGs except for C_{3v} . One common feature of these PGs is that each of the three Cartesian axes shows at least one of the n -fold rotational ($n \geq 2$) and reflection symmetries upon applying the \mathbf{m} . For example, for C_{4v} , the reflection \mathcal{M}_x (reflection plane yz) and \mathcal{M}_y (reflection plane xz) are maintained, respectively, with \mathbf{m} along x (i.e., [100]

TABLE I. Anomalous Hall conductivity tensor components of three-dimensional point groups that allow PAHE. The tensor is defined as $J_i = \sigma_{ij} E_j$ where J_i and E_j are the i th and j th components of Hall current \mathbf{J} and electric field \mathbf{E} , respectively. The Cartesian axes x , y , and z for each crystal system follow the convention used in Ref. [15] and summarized in the SM [16]. The PAHE components of the D_3 , C_{3v} , and D_{3d} PGs depend on the relative positions of the symmetry operations (rotational axis and reflection plane) and Cartesian axes. However, the symmetry restrictions on the tensor are the same. Thus we employ such coordinate sets that one of the in-plane twofold rotational axes is along x for D_3 and D_{3d} , and one of the reflection planes is parallel to xz plane for C_{3v} . More information can be found in Ref. [16].

Crystal system	Point group	Direction of \mathbf{m}		
		x	y	z
Hexagonal	C_{6h}	σ_{zx}	σ_{yz}	
	C_{3h}	σ_{zx}	σ_{yz}	
	C_6	σ_{zx}	σ_{yz}	
Trigonal	D_{3d}		σ_{xy}	
	C_{3v}	σ_{xy}		
	D_3		σ_{xy}	
	C_{3i}	σ_{xy}, σ_{zx}	σ_{xy}, σ_{yz}	
Tetragonal	C_3	σ_{xy}, σ_{zx}	σ_{xy}, σ_{yz}	
	C_{4h}	σ_{zx}	σ_{yz}	
	S_4	σ_{zx}	σ_{yz}	
Monoclinic	C_4	σ_{zx}	σ_{yz}	
	C_{2h}	σ_{xy}		σ_{yz}
	C_s	σ_{xy}		σ_{yz}
Triclinic	C_2	σ_{xy}		σ_{yz}
	C_i	σ_{xy}, σ_{zx}	σ_{xy}, σ_{yz}	σ_{yz}, σ_{zx}
	C_1	σ_{xy}, σ_{zx}	σ_{xy}, σ_{yz}	σ_{yz}, σ_{zx}

direction) and y (i.e., $[010]$ direction). For D_{3h} , the twofold rotational symmetry along the in-plane lattice vector \mathbf{a} (i.e., x) is preserved with \mathbf{m} along x and the reflection symmetry \mathcal{M}_y (reflection plane xz) is preserved with \mathbf{m} along y . The synergy of these remaining rotational/reflection symmetries prohibits the PAHE in the PGs mentioned above. However, if there is at least one axis that shows no rotational and reflection symmetry upon applying \mathbf{m} , the PAHE is allowed, which comprise Table I. Let's take D_3 as an example. We take one of the twofold rotational axes along the x direction (i.e., along in-plane lattice vector \mathbf{a} [16]). No rotational symmetry is maintained when \mathbf{m} is along y but the twofold rotational symmetry along x is maintained when \mathbf{m} is along x . As a result, PAHE is allowed with \mathbf{m} along y in D_3 .

The above discussions establish for PAHE the preconditions of breaking both rotational and reflection symmetries. But it is still not clear about the plane in which the PAHE appears. By analyzing the symmetries upon applying \mathbf{m} , we find that, while the reflection (rotational) symmetry is broken when \mathbf{m} is in the reflection plane (the plane perpendicular to the rotational axis), the combination of reflection \mathcal{M} (twofold rotation C_2) and time-reversal symmetry \mathcal{T} , i.e., \mathcal{MT} ($C_2\mathcal{T}$), is maintained. Such combinations of \mathcal{MT} and $C_2\mathcal{T}$ import additional restrictions for the AHE. Let's consider the most interesting in-plane component σ_{xy} (similar discussion below can be applied to the other components). For example, for C_{3h} PG as shown in Table I, the PAHE is only allowed when \mathbf{m} lies in the xy plane. However, due to the maintained \mathcal{MT} (\mathcal{M} here is the reflection σ_h along z axis), the AHE in the xy plane (σ_{xy}) is forbidden. For C_n PG (n is even), now the $C_2\mathcal{T}$ plays the role of \mathcal{MT} in C_{3h} . Similar discussions can be performed for other PGs. In short, the in-plane AHE is not allowed in the PGs with either even-fold rotational symmetry (the rotational axis is along z direction) or σ_h reflection when \mathbf{m} lies in the xy plane.

Now we discuss the 2D case. Previous works [7–10] revealed the possibility to realize in-plane quantized AHE effect with in-plane magnetization on the precondition of breaking all the reflection symmetries. However, rotational symmetry has not been well considered before. This may be because the materials or models considered therein have no twofold rotational and reflection symmetries along the out-of-plane direction and thus do not suffer from $C_2\mathcal{T}$ or \mathcal{MT} with in-plane magnetization. Here we emphasize the role played by $C_2\mathcal{T}$ and \mathcal{MT} and conclude that the PAHE can never happen in *pure* 2D cases with in-plane magnetization (regardless of the stability of such a magnetization). But the PAHE can happen with in-plane magnetization in the 2D PGs of C_1/C_3 and D_1/D_3 with the prerequisite of breaking σ_h reflection, e.g., by a slight buckling of the plane.

While the above discussions for the 2D case with in-plane magnetization are robust, we have to emphasize the arguments for 3D PGs are based on the assumption that the magnetization \mathbf{m} is along the specified high-symmetry directions. If \mathbf{m} is misaligned to the high-symmetry direction that destroys all the rotational and reflection symmetries as well as the combinations \mathcal{MT} and $C_2\mathcal{T}$, then PAHE can show up in any crystal class. Such a symmetry-breaking process can be realized by either an external magnetic field \mathbf{H} along a general direction or a particular type of intrinsic

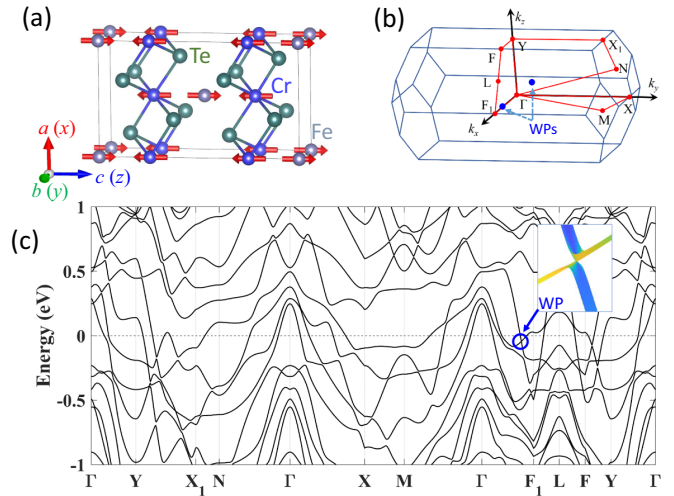


FIG. 2. Crystal and band structures of FeCr_2Te_4 . (a) Crystal and magnetic structure of FeCr_2Te_4 with the red vectors on Cr and Fe atoms showing the experimentally confirmed ferrimagnetic configuration, where the local moments are aligned ferromagnetically along the c axis in each sublattice but antiferromagnetically aligned between the two sublattices. (b) The first Brillouin zone of the primitive cell together with the high-symmetry points used in (c) are shown. The blue dots represent a pair of Weyl points near the Fermi level. (c) The band structure under the experimental ferrimagnetic configuration including SOC (the energy is referenced to the Fermi level). The band crossing on ΓF_1 at the energy of -44 meV forms a type-I Weyl point (WP) and the inset shows the dispersion relation near the WP on the k_x - k_y plane. Yellow (blue) color stands for higher (lower) band weight of Fe.

magnetization. In addition, though based on the magnetization from the ferromagnetic configuration, our symmetry considerations are also applicable to other magnetic configurations such as antiferromagnetic configuration and noncollinear magnetic configuration.

IV. MATERIAL PREDICTION

We now demonstrate by first-principles calculation the PAHE in the ferrimagnetic Weyl semimetal FeCr_2Te_4 , which has been reported recently about the ferrimagnetism and general AHE from experiment [17,18]. The crystal structure of FeCr_2Te_4 , as shown in Fig. 2(a), can be regarded as the Fe-intercalated AA-stacking of the 1T phase of a transition-metal dichalcogenide (CrTe_2) with distortions. It has a monoclinic structure with a space group of $I2/m$ (C_{2h}), and the angle between the lattice vectors \mathbf{a} and \mathbf{c} is 90.01° (the small deviation from 90° will be ignored below). The twofold rotational symmetry C_2 is along lattice vector \mathbf{b} and reflection \mathcal{M} is with respect to the \mathbf{ac} plane. The experimentally confirmed ferrimagnetic configuration with the easy axis along c is shown in Fig. 2(a). Within such a magnetic configuration, both the C_2 and \mathcal{M} are broken but the combined $C_2\mathcal{T}$ and \mathcal{MT} symmetries are maintained.

The Perdew-Burke-Ernzerhof [19] level band structure, as calculated by the density functional theory as implemented in VIENNA AB INITIO SIMULATION PACKAGE [20,21], is shown in Fig. 2(c) where SOC is included. FeCr_2Te_4 is metallic, which

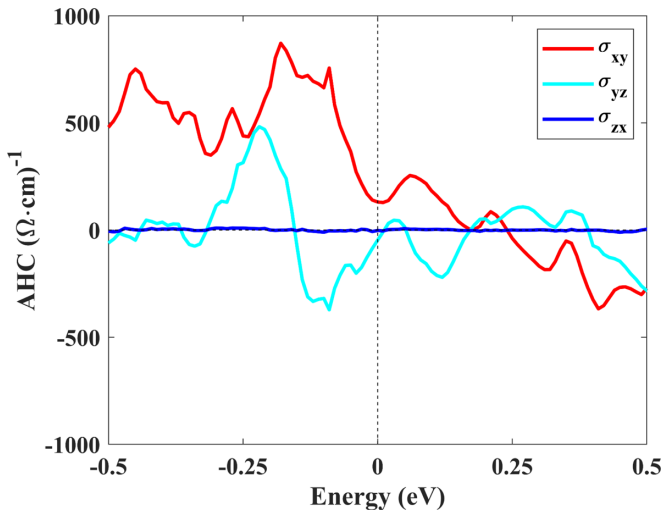


FIG. 3. Anomalous Hall conductivity (AHC) of FeCr_2Te_4 under the experimental ferrimagnetic configuration. The energy is relative to the Fermi energy.

is different from its isostructural FeCr_2Se_4 , who is an antiferromagnetic insulator [22,23]. There are many band-crossing points in the band structure, some of which are potential WPs. For example, by employing WANNIERTOOLS software [24], we identify that the band crossing point on ΓF_1 at -44 meV is a type-I WP as shown in Fig. 2(c). Due to the maintained inversion symmetry, there is another WP corresponding to the one on ΓF_1 . The positions of this pair of WPs in the Brillouin zone are shown in Fig. 2(b) by blue dots. Such WPs (and other band crossing points) generally contribute much to the Berry curvature and thus to the intrinsic AHC who is the integral of Berry curvature over all the occupied bands. But be aware that the WP is not a prerequisite of AHE according to the symmetry analyses above.

Based on a tight-binding Hamiltonian as obtained with the maximally localized Wannier functions [25], we calculate the intrinsic AHC by using the Kubo formula approach. Figure 3 shows the calculated AHC under the experimental ferrimagnetic configuration. The component σ_{xy} (magnetization along z), which represents the general AHE, shows a value of about $130 (\Omega \times \text{cm})^{-1}$ at the Fermi energy. This intrinsic AHC is larger than the experimental value where the extrinsic contribution dominates the AHE of FeCr_2Te_4 as discussed in literature [18]. Here we focus on the intrinsic part. While the experiment had reported the σ_{xy} , the PAHE has not been reported. According to our calculation, the most intriguing component σ_{yz} , where the electric field or the Hall current is in the same direction of the intrinsic magnetization (i.e., z direction), is nonzero, which confirms our above proposal of the PAHE as depicted in Figs. 1(b) and 1(c). The WP shown in

Fig. 2(c) is accidental and not a prerequisite for PAHE (σ_{yz}). The value of σ_{yz} at the Fermi energy is $\sim 50 (\Omega \times \text{cm})^{-1}$, in the same order of σ_{xy} . If the system is slightly doped by a hole, σ_{yz} can even reach a value of as large as $500 (\Omega \times \text{cm})^{-1}$. The σ_{zx} is always zero because of the maintained $C_2\mathcal{T}$ and \mathcal{MT} symmetries.

V. EXPERIMENTAL SIGNATURE

Very recently, the in-plane AHE was reported in the potential Dirac or Weyl semimetal material ZrTe_5 [26] when the in-plane magnetic field \mathbf{H} is parallel and perpendicular to the electric field \mathbf{E} . ZrTe_5 has a PG of D_{2h} . According to the symmetry analyses above, this PG does not show PAHE when the \mathbf{H} is along any of the three crystallographic directions since there are always a reflection symmetry and a twofold rotational symmetry left. However, in experiments, the electrodes are misaligned with the in-plane lattice vectors \mathbf{a} as manifested in the literature. This misalignment leads to the misalignment between \mathbf{H} and the in-plane \mathbf{a} or \mathbf{c} axes when \mathbf{H} is parallel or perpendicular to \mathbf{E} , and thus breaks all the symmetry restrictions for PAHE we proposed above. Thus, we think the antisymmetric part of the measured unconventional AHE is a signal of PAHE. This actually goes to the proposal above where \mathbf{H} is applied along a general direction for realizing PAHE.

VI. CONCLUSION

We have explored the possibility of realizing an unconventional AHE—PAHE—where the magnetization (or magnetic moment) is coplanar with the electric field and the Hall current. By symmetry analyses, we reveal that breaking the rotational and reflection symmetries is critical for realizing PAHE in 3D. For 2D cases, in addition to the above prerequisites, breaking the additional combinations of twofold rotational symmetry C_2 , reflection symmetry \mathcal{M} (both along out-of-plane direction), and time-reversal symmetry \mathcal{T} (i.e., $C_2\mathcal{T}$ and \mathcal{MT}) is also essential. By first-principles calculation, we demonstrate this unconventional AHE in a realistic ferrimagnetic Weyl semimetal. Our symmetry discussions also apply to the conventional Hall effect.

ACKNOWLEDGMENTS

We thank Cedimir Petrovic and Daniel Kaplan for inspiring discussions. B.Y. acknowledges the financial support by the Willner Family Leadership Institute for the Weizmann Institute of Science, the Benozio Endowment Fund for the Advancement of Science, Ruth and Herman Albert Scholars Program for New Scientists, and the European Research Council (ERC) under the European Union's Horizon 2020 research and innovation program (Grant No. 815869).

- [1] N. Nagaosa, J. Sinova, S. Onoda, A. H. MacDonald, and N. P. Ong, Anomalous Hall effect, *Rev. Mod. Phys.* **82**, 1539 (2010).
 [2] D. Xiao, M.-C. Chang, and Q. Niu, Berry phase effects on electronic properties, *Rev. Mod. Phys.* **82**, 1959 (2010).

- [3] S. Nakatsuji, N. Kiyohara, and T. Higo, Large anomalous Hall effect in a non-collinear antiferromagnet at room temperature, *Nature (London)* **527**, 212 (2015).
 [4] A. K. Nayak, J. E. Fischer, Y. Sun, B. Yan, J. Karel, A. C. Komarek, C. Shekhar, N. Kumar, W. Schnelle,

- J. Kübler, C. Felser, and S. S. P. Parkin, Large anomalous Hall effect driven by a nonvanishing Berry curvature in the noncollinear antiferromagnet Mn_3Ge , *Sci. Adv.* **2**, e1501870 (2016).
- [5] H. Chen, Q. Niu, and A. H. MacDonald, Anomalous Hall Effect Arising from Noncollinear Antiferromagnetism, *Phys. Rev. Lett.* **112**, 017205 (2014).
- [6] Y. Zhang, Y. Sun, H. Yang, J. Železný, S. P. P. Parkin, C. Felser, and B. Yan, Strong anisotropic anomalous Hall effect and spin Hall effect in the chiral antiferromagnetic compounds Mn_3X ($X = Ge, Sn, Ga, Ir, Rh, \text{ and } Pt$), *Phys. Rev. B* **95**, 075128 (2017).
- [7] X. Liu, H.-C. Hsu, and C.-X. Liu, In-Plane Magnetization-Induced Quantum Anomalous Hall Effect, *Phys. Rev. Lett.* **111**, 086802 (2013).
- [8] Y. Ren, J. Zeng, X. Deng, F. Yang, H. Pan, and Z. Qiao, Quantum anomalous Hall effect in atomic crystal layers from in-plane magnetization, *Phys. Rev. B* **94**, 085411 (2016).
- [9] P. Zhong, Y. Ren, Y. Han, L. Zhang, and Z. Qiao, In-plane magnetization-induced quantum anomalous Hall effect in atomic crystals of group-V elements, *Phys. Rev. B* **96**, 241103(R) (2017).
- [10] Z. Liu, G. Zhao, B. Liu, Z. F. Wang, J. Yang, and F. Liu, Intrinsic Quantum Anomalous Hall Effect with In-Plane Magnetization: Searching Rule and Material Prediction, *Phys. Rev. Lett.* **121**, 246401 (2018).
- [11] H. X. Tang, R. K. Kawakami, D. D. Awschalom, and M. L. Roukes, Giant Planar Hall Effect in Epitaxial (Ga,Mn)As Devices, *Phys. Rev. Lett.* **90**, 107201 (2003).
- [12] A. A. Burkov, Giant planar Hall effect in topological metals, *Phys. Rev. B* **96**, 041110(R) (2017).
- [13] S. Nandy, G. Sharma, A. Taraphder, and S. Tewari, Chiral Anomaly as the Origin of the Planar Hall Effect in Weyl Semimetals, *Phys. Rev. Lett.* **119**, 176804(R) (2017).
- [14] R. Battilomo, N. Scopigno, and C. Ortix, Anomalous planar Hall effect in two-dimensional trigonal crystals, *Phys. Rev. Res.* **3**, L012006 (2021).
- [15] *IEEE Standards on Piezoelectric Crystals*, chaired by J. G. Brainerd (IEEE, 1949), pp. 1–20.
- [16] See Supplemental Material at <http://link.aps.org/supplemental/10.1103/PhysRevB.103.214438> for more details.
- [17] Y. Liu, R. J. Koch, Z. Hu, N. Aryal, E. Stavitski, X. Tong, K. Attenkofer, E. S. Bozin, W. Yin, and C. Petrovic, Three-dimensional Ising ferrimagnetism of Cr-Fe-Cr trimers in $FeCr_2Te_4$, *Phys. Rev. B* **102**, 085158 (2020).
- [18] Y. Liu, H. Tan, Z. Hu, B. Yan, and C. Petrovic, Anomalous Hall effect in the weak-itinerant ferrimagnet $FeCr_2Te_4$, *Phys. Rev. B* **103**, 045106 (2021).
- [19] J. P. Perdew, K. Burke, and M. Ernzerhof, Generalized Gradient Approximation Made Simple, *Phys. Rev. Lett.* **77**, 3865 (1996).
- [20] G. Kresse and J. Furthmüller, Efficient iterative schemes for *ab initio* total-energy calculations using a plane-wave basis set, *Phys. Rev. B* **54**, 11169 (1996).
- [21] G. Kresse and J. Furthmüller, Efficiency of *ab-initio* total energy calculations for metals and semiconductors using a plane-wave basis set, *Comput. Mater. Sci.* **6**, 15 (1996).
- [22] G. J. Snyder, T. Caillat, and J.-P. Fleurial, Thermoelectric, transport, and magnetic properties of the polaron semiconductor $Fe_xCr_{3-x}Se_4$, *Phys. Rev. B* **62**, 10185 (2000).
- [23] B. I. Min, S. S. Baik, H. C. Choi, S. K. Kwon, and J. S. Kang, Electronic structures of magnetic semiconductors $FeCr_2Se_4$ and $Fe_{0.5}Cu_{0.5}Cr_2Se_4$, *New J. Phys.* **10**, 055014 (2008).
- [24] Q. S. Wu, S. N. Zhang, H.-F. Song, M. Troyer, and A. A. Soluyanov, Wanniertools: An open-source software package for novel topological materials, *Comput. Phys. Commun.* **224**, 405 (2018).
- [25] N. Marzari, A. A. Mostofi, J. R. Yates, I. Souza, and D. Vanderbilt, Maximally localized Wannier functions: Theory and applications, *Rev. Mod. Phys.* **84**, 1419 (2012).
- [26] J. Ge, D. Ma, Y. Liu, H. Wang, Y. Li, J. Luo, T. Luo, Y. Xing, J. Yan, D. Mandrus *et al.*, Unconventional Hall effect induced by Berry curvature, *Natl. Sci. Rev.* **7**, 1879 (2020).